Singularities in Surface Waves

G. Ruíz Chavarría and T. Rodriguez Luna

Abstract In this paper we investigate the evolution of surface waves produced by a parabolic wave maker. This system exhibits, among other, spatial focusing, wave breaking, the presence of caustics and points of full destructive interference (dislocations). The first approximation to describe this system is the ray theory (also known as geometrical optics). According to it, the wave amplitude becomes infinite along a caustic. However this does not happen because geometrical optics is only an approximation which does not take into account the wave behavior of the system. Otherwise, in ray theory the wave breaking does not hold and interference occurs only in regions delimited by caustics. A second step is the use of a diffraction integral. For linear waves this task has been made by Pearcey (1946) (Pearcey, Philos Mag 37 (1946) 311–317) for electromagnetic waves. However the system under study is non linear and some features have not counterpart in the linear theory. In the paper our attention is focused on three types of singularities: caustics, wave breaking and dislocations. The study we made is both experimental and numerical. The experiments were conducted with two different methods, namely, Schlieren synthetic for small amplitudes and Fourier Transform Profilometry. With respect the numerical simulations, the Navier-Stokes and continuity equations were solved in polar coordinates in the shallow water approximation.

1 Introduction

Waves are ubiquitous in nature. The light and the sound are two examples of them, but possibly the most classical picture is that of a wave on the surface of a liquid. They carry energy but not mass and exhibits a myriads of phenomena like reflection, refraction, interference and diffraction. The linear waves are by far the most studied due to the fact that its properties can be deduced analytically. Usually a wave is represented as having a sinusoidal shape, with constant amplitude and a defined

G. Ruíz Chavarría (✉) · T. Rodriguez Luna
Facultad de Ciencias, Universidad Nacional Autónoma de México, Ciudad Universitaria, 04510 Mexico, D.F., Mexico
e-mail: gruiz@unam.mx

J. Klapp et al. (eds.), *Selected Topics of Computational and Experimental Fluid Mechanics*, Environmental Science and Engineering,
DOI 10.1007/978-3-319-11487-3_12

wavelength, however this is just an idealized image. Most of times the wave field contains a continuum of wavelengths, so its shape takes a complicated form and often it evolves in time. This paper deals with waves on the surface of a liquid, which are governed by the Navier-Stokes and continuity equations. They share some features with linear waves, but some of its properties are the result of nonlinear interactions. An example is the waveform, which is no more symmetric as in a sinusoidal wave. On the other side, the amplitude of a surface wave cannot grow indefinitely, after a threshold the wave breaks. The energy carried is rapidly dissipated into turbulence, the formation of air bubbles and drops, etc. (Babanin 2011). This phenomenon is commonly observed along the coasts, when the waves approach the shore. Under these circumstances the wave amplitude grows essentially by a decrease in the sea depth, until the slope of surface becomes infinite. This is the bathymetric breaking, which has been studied extensively. In the open sea the wave breaking is also present, but the mechanisms involved in its production are quite different. Let us consider a continuous wave field and the fact that surface waves are dispersive. Then, components of different wavelengths moves with different phase velocity. The further evolution could produce a rise in the wave amplitude and eventually to the development of the breaking. Of course there are others mechanisms involved in the wave breaking, among them, the interaction between the wind and the waves and the occurrence of currents moving in opposite direction to the wave motion (Zemenzer 2009).

In the ocean there are three stages in the wave evolution (Babanin 2011). In the first one the wind blows and deforms the water-air interface, so an initially small amplitude wave is produced. During a time scale covering thousand of periods energy is injected to the wave, allowing to a slow growth of its amplitude. In this step the wave evolution can be described with a weak nonlinear theory. In the second stage, which covers only few periods, the wave becomes highly asymmetric either in the horizontal and vertical directions. The peaks become steeper and the troughs retract. At a certain time the free surface becomes multivaluated and breaking develops just in a fraction of a period. The breaking is the mechanism to dissipate energy, which is converted in heat, turbulence, bubble production, etc. The case we study has a different driving mechanism, namely the spatial focusing. The aim to make experiments with this kind of breaking is to study this phenomenon in laboratory, where waves cannot evolve over thousand of wavelengths, but in which underlying nonlinear interactions are still present. In addition the study of the wave field under spatial focusing reveals the existence of other singularities apart breaking, like caustics and dislocations, and phenomena as interference and diffraction.

As stated before a nonlinear wave is asymmetric. In order to quantify this asymmetry two quantities are introduced, the skewness and the asymmetry, defined as (Babanin 2011):

$$S = \frac{a_1}{a_2} - 1, \tag{1}$$

$$A_s = \frac{b_1}{b_2} - 1, \tag{2}$$

where a_1 is the amplitude of the peak, a_2 is the amplitude of the trough, b_1 is the distance from the peak to the next point of zero amplitude, and b_2 is the distance from the peak to the previous point of zero amplitude. For a linear wave both quantities vanish. In a nonlinear wave the first one is positive while the second one is negative.

Most of analytical results about surface waves have been obtained when the amplitude is small and consequently non linear terms are neglected in the governing equations. In addition, another hypothesis are made, namely, the velocity field is assumed irrotational and viscosity is neglected. Under all these assumptions, it is possible to derive a dispersion relation, which in the general case is given by the following equation (Elmore and Heald 1969):

$$\omega^2 = \left(gk + \frac{\sigma k^3}{\rho}\right)\tanh(kH), \tag{3}$$

where k is the wavenumber, σ the surface tension coefficient, ρ the fluid density and H is the liquid depth. In the limit of deep waters ($\lambda \ll H$) the term $\tanh(kH) \approx 1$. Then, waves are dispersive, that is, the phase velocity $c = \omega/k$ is dependent on the wavenumber k. The opposite limit is the shallow water case ($\lambda \gg H$) for which the phase velocity is $c = \sqrt{gH}$, irrespective the wavelength.

In Fig. 1 the phase velocity for waves in the deep water approximation is plotted as a function of the wavelength λ. The wavelength lies in the range 1–200 cm. In the figure it is clear that waves are dispersive and that phase velocity attains a minimal value for $\lambda = 2\pi\sqrt{\frac{\sigma}{\rho g}} = 1.70$ cm. It is important to note that the dependence of phase velocity on wavelength in deep waters is a key feature for the time focusing.

This paper is organized as follow. Section 2 is devoted to describe the wave field produced by a parabolic wave maker, the ray theory, the theories of Airy and Pearcey and the singularities in this wave field (caustics and dislocations). In Sect. 3 we describe the optical methods to study surface waves and the experimental setup. In

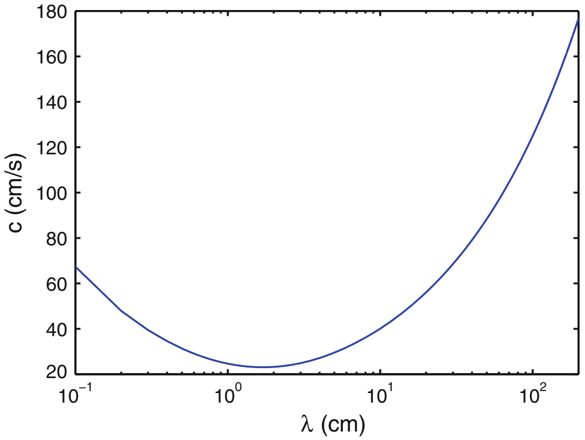

Fig. 1 Phase velocity (c) of surface wave versus wavelength (λ) in the deep water approximation ($\lambda \ll H$). The phase velocity depends upon the wavelength. In experiments and numerical simulations, the wavelength lies in the range $1 < \lambda < 10$ cm

Sect. 4 the numerical method, valid in shallow water approximation, is presented. The main results are presented in Sect. 5, in particular, the emergence of wave breaking, the behavior of the waves around caustics, the existence of dislocations and the recovery of a linear behavior far from the caustics. Finally in Sect. 6 the conclusion are drawn.

2 Spatial Focusing, Caustics and Dislocations

In order to give a picture of the spatial focusing let us consider that surface waves are produced by a parabolic wave maker. The equation of a parabola is:

$$y_0 = a x_0^2. \tag{4}$$

The first approximation in the study of this wave field is the use of geometrical optics, that is, it is assumed that rays start in the parabola and move perpendicular to it. The wave fronts—as shown in Fig. 2—are obtained by a knowledge of normal vector at each point of the parabola. As it can be seen, in the vicinity of the parabola the size of wavefronts decrease as the wave progresses, that implies a growth in the amplitude because energy must be conserved (the viscosity has been neglected). Locally the rays form a beam converging in the center of curvature of the parabola. For a point (x_0, y_0) lying in the parabola, the curvature is:

$$\kappa = \frac{2a}{\left(1 + 4a^2 x_0^2\right)^{3/2}}. \tag{5}$$

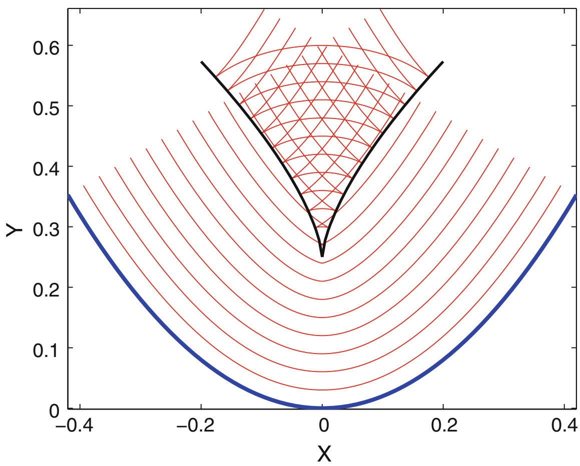

Fig. 2 Wave fronts produced by a parabolic wave maker. The *black lines* are caustics, which intersect in a point (Huygens cusp). The caustics can be considered as the locus where the wavefronts are folded and also as the *curves* where wave amplitude become infinite according to ray theory. Focusing is evident if we consider that size of wave fronts reduces before the Huygens cusp

The radius of curvature is the inverse of κ ($\rho_c = 1/\kappa$). The method of stationary phase allows us to obtain an expression for the wave amplitude in terms of the distance traveled (d) by the ray and ρ (Paris and Kaminsky 2001):

$$A = A_0 \sqrt{\frac{\rho_c}{\rho_c - d}}, \tag{6}$$

where A_0 is the initial amplitude. The last equation predicts that amplitude diverge for $d = \rho_c$. The curve (or the surface in 3D waves) where optical geometry predicts the divergence of wave amplitude is known as a caustic. In reality this does not happen because ray theory is only an approximation in which the wave properties are not considered. However, along a caustic we have a bright region (we use the terminology of optics). In our system, we deal with a pair of caustics intersecting in a point. This point is known as Huygens cusp and around it maximal wave amplitudes take place. The equation of the caustics is:

$$x = \pm \frac{4}{3} \sqrt{\frac{a}{3}} \left(y - \frac{1}{2a} \right)^{\frac{3}{2}}. \tag{7}$$

It is interesting to remark that other characteristics can be invoked for the definition of a caustic. Note that along the caustic the wave fronts folds. This means that caustic is the line (surface) separating illuminated from shaded regions. In this sense, a caustic is the envelope of a ray family. An alternative definition of caustic follows from Fig. 3, in which some rays originating in wave maker have been drawn. The caustic separates region I, where only an individual ray reaches each point, from region II, where three rays reach each point.

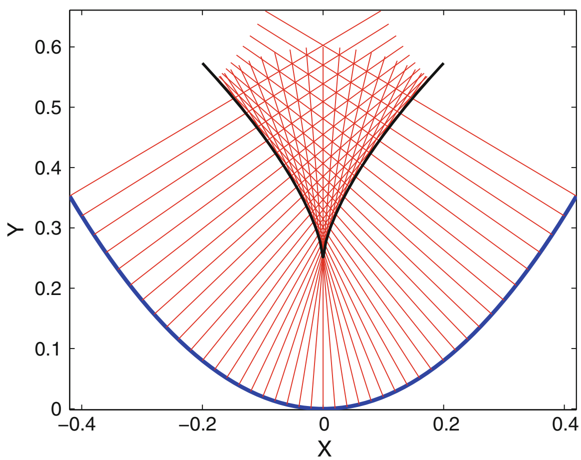

Fig. 3 Rays originating in the parabolic wavemaker. In region I only a ray passes through a point, while in region II three rays reach each point. The *curve* separating both regions is again the caustics

In region II occur some wave phenomena, noticeably, the interference. The presence of three rays give rise to the appearance of points where fully destructive interference happens. This points are called dislocations because of its similarity with dislocations in a crystal lattice. This kind of object is a true singularity, where the phase becomes undefined. It is important to stress that dislocations appear not only in the illuminated region, but a line of dislocations occur in the dark zone because of the diffraction.

As we have stated before, the geometrical optics fails to predict the behavior in the vicinity of a caustic. The divergence has been overcome for the first time with the formulation of a theory by Airy in 1838. In order to describe the wave field near a caustic Airy introduced a function called in his honor, which have some important properties related to the existence and the absence of rays in both sides of a caustic. This function is the solution of the differential equation:

$$\frac{d^2w}{dz^2} = zw. \tag{8}$$

The Airy function has a oscillating behavior for $z < 0$ and for $z > 0$ the function decays exponentially. It is important to mention that this theory is intended for simple caustic, that is, if only two rays reach each point in the illuminated region. The wave field produced by a parabolic wave maker differs from those studied by Airy because in the illuminated region, the wave is the result of the interference of three rays. The behavior of a linear wave in this configuration has been obtained by Pearcey (1946). The work of Pearcey is based in the use of a diffraction integral, which is an approximate solution of the wave equation. This integral is:

$$h(x, y) = \int_{-\infty}^{+\infty} \frac{dx_0}{cos(\theta(x_0))} \frac{exp(ikd(x_0, x, y))}{\sqrt{d(x_0, x, y)}}, \tag{9}$$

where $\theta(x_0)$ is the angle between the tangent of parabola at point x_0 and the x axis. This quantity usually is small, implying that $cos(\theta(x_0)) \approx 1$. Because interest is focused in the behavior around the Huygens cusp (its coordinates are $\left(0, \frac{1}{2a}\right)$ we perform a Taylor expansion of $d(x_0, x, y)$ to first order around this position. The final results is known as the Pearcey integral:

$$h(x, y) = \frac{k}{i2\pi} \frac{exp(ikR)}{\sqrt{R}} \left(\frac{2R}{ka^2}\right)^{1/4} \int_{-\infty}^{+\infty} exp\left(i\left[t^4 + Ut^2 + Vt\right]\right) dt, \tag{10}$$

where $R = \frac{1}{2a}$, $U = 2\left(\frac{k}{2R}\right)^{1/2}(R - y)$ and $V = -\frac{2}{\sqrt{a}}\left(\frac{k}{2R}\right)^{3/4} x$. If the wave maker has a finite size and wavelength is not small when compared with R, the integral must be carried over a finite domain.

3 Optical Methods to Study Surface Waves

In the last decade two optical methods have been developed to detect the deformation of the free surface in liquids. Both exploit the emergence of high definition digital cameras. The first one, known as synthetic Schlieren (Moisy et al. 2009), is based in the refraction of light and the second one, named Fourier transform profilometry (Cobelli et al. 2009; Maurel et al. 2009), is based in the reflection of light. In the two cases a full reconstruction of the free surface topography is realized, but they differ in the range of wave amplitudes they can measure. The underlying principle of synthetic Schlieren is the same used to detect density fluctuations inside a transparent fluid, that is, the change in the light trajectory due to variations in the refraction index. Consider a ray that starts at the bottom of a liquid layer and moves to the liquid-air interface. The trajectory followed by the ray satisfies the Snell law. If the surface is deformed, incidence angle is modified and consequently refraction angle is also modified. For the implementation of this method a set of dots randomly distributed is put at the bottom of the fluid. In a first step a snapshot of the dots pattern is recorded when free surface is flat, this is called the reference image. In a second step, an image is taken when the wave progresses. Due to the modification of the incidence angle, related to the deformation of the liquid-air interface, an apparent displacement of dots appear when we compare first and second images. If we assume that deformations are small (compared with wavelength) and if we remain in the paraxial approximation, the apparent displacement δr is proportional to the gradient of the free surface, namely (Moisy et al. 2009):

$$\nabla h = -\frac{\delta r}{h^*}, \tag{11}$$

where $\frac{1}{h^*} = \frac{1}{\alpha H} - \frac{1}{L}$, H is the depth layer, L is the distance to the camera to the bottom ow liquid layer and α is the related to the ratio of the refractive indices, that is $\alpha = 1 - \frac{n'}{n}$. The determination of δr is performed with a PIV software. To this end the digital image is divided in small cells, where a cross correlation is made between actual image and the reference one. The reconstruction of the topography of free surface is made through the integration of the gradient field. The number of equations is twice the number of unknowns, so the system is overdetermined. For this reason, solution is made with a technique of least square. This method works well for small deformations. This fact limits the use of the method for cases where non linearity are still weak, however it allows the investigation of phenomena like diffraction or the appearance of dislocations in the dark side of caustics. A method better suited for the study of non linear waves is the Fourier transform profilometry (PTF). This procedure is based on light reflection. If we are interested in the study of waves in a fluid, the liquid must remain opaque to produce diffuse reflection. In order to implement it a pattern of fringes is projected on the liquid surface with the aid of a high definition video projector. The size of images is 1,920 × 1,080 pixels, it has depth of 12 bits per color and its intensity is 2,000 lumens. Images of the fluid surface are recorded with a digital camera using a raw format to avoid lost of information due to preprocessing. We have used a Fujifilm digital camera Finepix HS50 EXR, with a maximal resolution of 4,608 × 3,456 pixels, capable of recording images with 16 bits per color, which are after converted to a readable format. As in the synthetic Schlieren method, PFT require a comparison of digital images. In a first step, we take a snapshot of the fringe pattern when liquid surface is at rest. The second step consists in taking an image of the fringe pattern when the wave is present. Information of h is contained in the phase difference between two images. There are several possible configurations to arrange the camera and the video projector. In our experiments, axis of the camera and video projector are parallel. The relation between h and the phase difference $\Delta\phi$ is (Cobelli et al. 2009; Maurel et al. 2009):

$$h = \frac{\Delta\phi L}{\Delta\phi - \frac{2\pi}{p} D}, \tag{12}$$

where L is the distance of camera to liquid surface, D is the distance between lenses of camera and video projector and p is the wavelength of the fringe pattern. In an ideal case only two images are required to reconstruct the waveform. In reality we need to subtract undesirable factors, then corrections must be incorporated. Let us project on the liquid surface an image in which all pixels have the same intensity level. When this pattern is recorded with the digital camera, intensity is not constant. This is due, among other things, to the fact that when light reaches the liquid surface three phenomena take place, that is, reflection, transmission and absorption. The amount of energy carried by the reflected light is dependent on the incidence angle. In order to remove this source of undesirable effects we need also to record this kind of images and include them in the process for determining phase difference.

3.1 Experimental Setup

Experiments were carried out in a basin made in plexiglass whose dimensions are 120 cm × 50 cm × 15 cm. Waves were produced with a parabolic wave maker whose parameter a is 2 (see Eq. 4) and has 42 cm wide. The wave maker is connected to a mechanical vibrator which produces a sinusoidal motion of frequencies lying in the range 4–10 Hz, corresponding to wavelengths between 2.4 and 10 cm. The water level is set to 10 cm for both synthetic Schlieren and FTP experiments. The deep water approximation is well fulfilled because in all cases $\tanh(kH) > 0.999$. Images for synthetic Schlieren method cover an area of 20 cm × 11.2 cm, they were recorded with a full HD digital camera. In each realization a film of 50 frames/s was taken during 50 s. Each film includes frames for both unperturbed and wavy surfaces. Individual images are extracted from the film through the use of the free software ffmpeg. Digital processing was performed with DPIVsoft software (Meunier and Leweke 2003), which allows to obtain the free surface gradient. Finally the reconstruction of the surface topography h(x, y) is made by a finite difference approximation for spatial derivatives of the surface gradient.

With respect the implementation of Fourier Transform Profilometry an opaque liquid surface is required. This is achieved by adding a concentrated white dye to the water. The fringe pattern projected on the free surface covers an area of 28 cm $\times$ 50 cm, which is sufficient to investigate wave field before and after the Huygens cusp. On the other hand, the distance from projector to liquid surface is L = 1.14 m, the distance D is 0.30 cm and wavelength of fringe pattern was p = 0.003 m (3 mm). In order to avoid the appearance of undesirable bright spot the image produced by the videoprojector was shifted with no deformation (a feature available in newer equipment) and additionally two crossed polarizers have been put on the lenses of camera and videoprojector. As stated before, we use a digital camera capable of recording in raw format. A further conversion of images to a standard format (tif images of 16 bits per color) was made and finally processing was made with routines written in matlab.

4 Numerical Method

The surface waves are governed by the Navier-Stokes and continuity equations. In recent decades many researches of surface waves were made through numerical codes, however there are some difficulties in its use, for instance, the domain of integration changes in time. In this work we present numerical results for surface waves in the shallow water approximation, that is, when liquid depth is much lower than the wavelength λ ($H \ll \lambda$). The choice of this approximation was made on the basis that the system remains 2D but at the same time non linearity is retained. The equations to solve are:

$$\frac{\partial u}{\partial t} + u\frac{\partial u}{\partial r} + \frac{v}{r}\frac{\partial u}{\partial \theta} - \frac{v^2}{r} = -g\frac{\partial h}{\partial r}, \tag{13}$$

$$\frac{\partial v}{\partial t} + u\frac{\partial v}{\partial r} + \frac{v}{r}\frac{\partial v}{\partial \theta} - \frac{uv}{r} = -\frac{g}{r}\frac{\partial h}{\partial \theta}, \tag{14}$$

$$\frac{\partial h}{\partial t} + \frac{1}{r}\left(\frac{\partial (rhu)}{\partial r} + \frac{\partial (hv)}{\partial \theta}\right) = -\frac{H}{r}\left(\frac{\partial (ru)}{\partial r} + \frac{\partial v}{\partial \theta}\right), \tag{15}$$

where u and v are the horizontal components of the velocity field, h is the free surface deformation and H is the depth of the liquid layer. In the deduction of these equations, the viscosity was neglected and the continuity equation and the kinematical condition have been used. The numerical method used for solving Eqs. (13)–(15) involves a centered second order finite differences for radial coordinate, a backward second order finite difference for time and a spectral code for θ coordinate. The numerical code cannot predict the wave breaking because this process implies that variable h

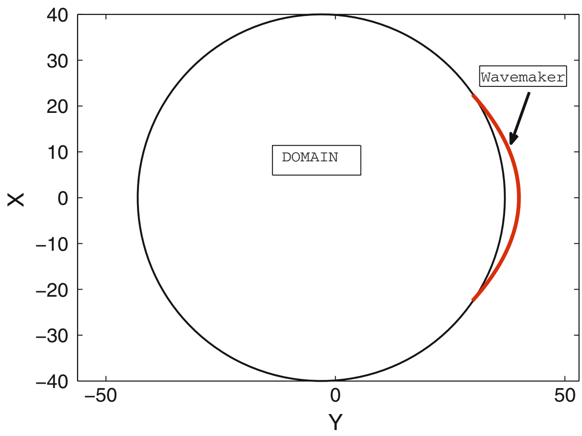

Fig. 4 Spatial domain used in the numerical solution. It is a annular ring ($r_1 < r < r_2$). The wave maker is outside this domain, it intersects the outer boundary in two points. The boundary conditions are set assuming that the wave front evolves according to the stationary phase method

become multivaluated. However it is possible to study the focusing and the emergence of nonlinearities appearing during the growth of waves. It is important to remark that when non linear terms are dropped from Eqs. (13)–(15) we recover the equations of a linear wave. The numerical solution is performed in a annular domain, for $r_1 < r < r_2$. The wave maker is outside this domain, it intersects the outer boundary in two points (see Fig. 4). We consider that initially the fluid is at rest, that is, surface is not deformed. For imposing the boundary conditions we approximate the values of surface deformation assuming that the wave evolve from wave maker to the outer boundary according to the stationary phase method. The numerical solution was carried out using a mesh of 400 points in radial direction and 256 modes in the angular variable θ. Otherwise the time step is set to $\delta t = 0.01$.

Numerical simulation was made under two conditions. In the first one the nonlinear terms are dropped, then solution correspond to a linear wave. In the second case nonlinear terms are retained. In both cases maximal amplitude is attained in the vicinity of Huygens cusp, along the symmetry axis. Otherwise, due to finite size of the wave maker we observe that interference in the region delimited by caustics occurs only in a section near the cusp.

5 Experimental and Numerical Results

As stated in Sect. 3 surface waves were produced with a parabolic wave maker. In order to characterize the initial wave front we recall that the equation of a parabola is $y_0 = ax_0^2$. In our experiments and in numerical simulations the value of parameter a is 2; thus the position of the Huygens cusp is $R = \frac{1}{2a} = 0.25$ m away from the parabola vertex. Most of results presented here correspond to waves with a frequency $f = 7$ Hz or equivalently $\lambda = 3.82$ cm. Experiments and numerical simulations were conducted to study three types of singularities: wave breaking, caustics and dislocations. Attention is paid to the growth of wave amplitude in the vicinity of the Huygens cusp, because in this region these singularities occur. On one side a non linear wave cannot rise indefinitely, at certain time the wave breaking begins. On the other side diffraction is capable to produce dislocations on the dark side of caustics. Some comments will be addressed to the decay of wave field far from the Huygens cusp and the recovery of the linear behavior far from caustics. In most of experiments the topography of the free surface is recovered with the method of Fourier Transform Profilometry. The images recorded by the digital camera cover only a fraction of the fringe pattern, but in any case we consider regions around the Huygens cusp. On the other side, experiments with synthetic Schlieren method were conducted covering an area of 20 cm $\times$ 11.2 cm. Images were taken at 4 different positions in the range $10 < y < 50$. The area covered in a position of the camera overlap with the next one, so we have a complete set of data in a region of 20 cm $\times$ 40 cm. In some cases it is best the use of synthetic Schlieren method. For instance, in a previous work this method has been successfully used to prove that for small amplitude waves (Ruiz-Chavarria et al. 2014) ($h < 10^{-4}$ m) the nonlinearities are already relevant. Another case were synthetic Schlieren method is suitable deals with the study of divergent waves because amplitude decreases as they progress. This happens in our system after passing the cusp.

Figure 5 shows the wave field as measured by the FTP method for a driving frequency of 7 Hz in the area delimited by $-11 < x < 11$ cm and $7 < y < 32$ cm. As in all figures in this paper, wave progresses from right to left. The Huygens cusp is located inside this region. Otherwise, the focusing becomes evident by two facts: (a) the size of wave front decreases from right to left and (b) the wave amplitude (represented by colors) grows when approaching the cusp. At the left border of figure

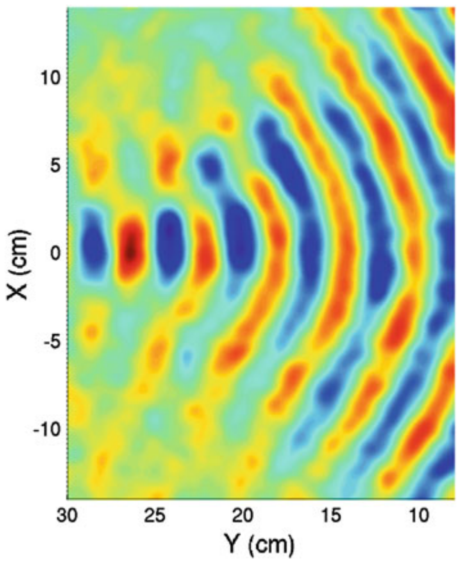

Fig. 5 Wave field of a monochromatic wave of f = 7 Hz produced by a parabolic wave maker. Wave progresses from *right* to *left*. In the figure the maximal amplitude occurs after passing the cusp

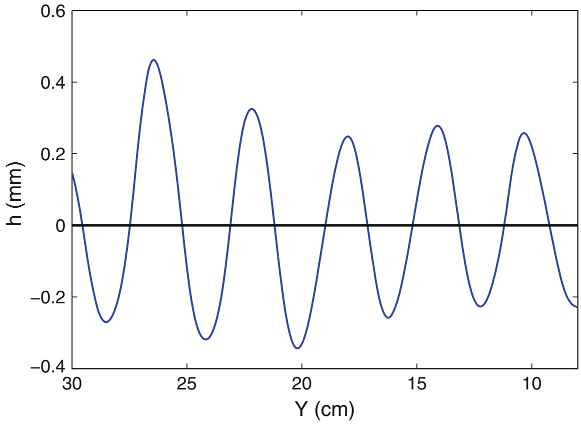

Fig. 6 Monochromatic wave of f = 7 Hz produced by a parabolic wave maker along the symmetry axis. Wave progresses from *right* to *left*. The asymmetry of the wave reveals that nonlinearities are important

there is a change of sign of the wavefront curvature, so waves become divergent. Consequently the further evolution leads to a decrease of the wave amplitude.

Taking into account that the maximal value of surface deformations occurs along x = 0, in Fig. 6 we show the curve h versus y along the symmetry axis. The maximal amplitude occurs at $y = 27$ cm, after passing the cusp, in agreement with results by Pearcey. A key feature of Fig. 6 is the asymmetry of the wave. This is a signature of a nonlinear behavior. For $y > 27$ cm the wave amplitude decreases because wave becomes divergent. In order to follow evolution of such divergent waves we have

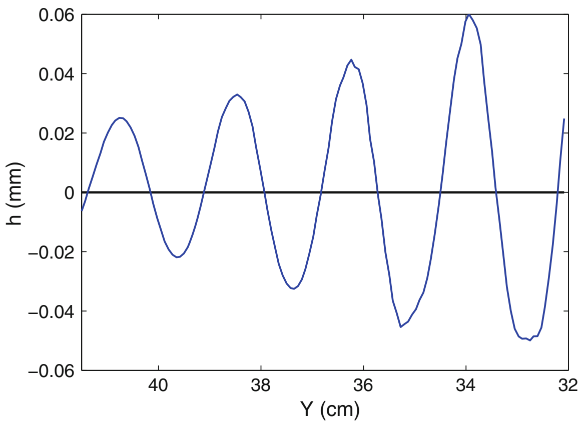

Fig. 7 Wave field of a monochromatic wave of f = 10 Hz produced by a parabolic wave maker. The topography of the free surface was obtained with the synthetic Schlieren method. Wave progresses from *right* to *left*. At y = 40 the values of skewness and asymmetry are respectively 0.06 and −0.02. At y = 34 cm these quantities take the following values $A_s = 0.16$ and $S = -0.04$

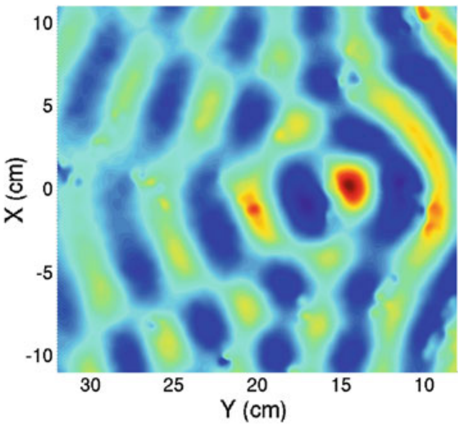

Fig. 8 Wave field in which breaking is developing. The wave frequency is 7 Hz. The amplitude increases monotonically before y = 15 cm. After this point the wave becomes divergent. During the wave breaking a fraction of the energy is dissipated

measured the free surface topography for $y > 30$ cm with the synthetic Shlieren method. The result presented in Fig. 7, corresponds to a wave of frequency f = 10 Hz ($\lambda = 2.4$ cm). An important feature is that, as wave progresses the amplitude decreases and nonlinear behavior weakens. In fact, skewness and asymmetry have the following values at y = 40 cm: $A_s = 0.06$ and $S = -0.02$, whereas the same quantities take the values $A_s = 0.16$ and $S = -0.04$ at y = 34 cm. This is a proof that far from the caustics the wave is well described by the linear theory.

In order to produce wave breaking, a higher amplitude is required. In Fig. 8 we show a snapshot of the wave field in which breaking develops. We remark two facts: (a) the nonlinear interactions lead to a greater ratio of maximal to initial amplitudes (the amplitude at the wave maker) when compared with results shown in Figs. 5, 6 and 7 and (b) the position of maximal wave amplitude is $y = 15$ cm, some wavelength before the Huygens cusp.The shape of the wave fronts is clearly modified by the breaking. First at all the wave appears as divergent for $y > 15$ cm. In addition, just before $y = 15$ cm the growth of wave develops rapidly over a distance comparable to a wavelength. In Fig. 9 the wave along the symmetry axis ($x = 0$) is shown. Before $y = 15$ cm the amplitude grows monotonically but after this point the wave exhibits important modifications. For instance the peaks located at $y = 26$ cm and $y = 30$ split in two local maxima. Finally it is important to say that the decrease of the amplitude during the breaking reveals that energy is dissipated.

Now we present some results of the numerical simulations. All the wave maker characteristics are retained and the driving frequency is again 7 Hz. In Fig. 10 we show snapshots of both linear (Fig. 10a) and nonlinear waves (Fig. 10b). For a linear wave the initial amplitude is irrelevant (only the ratio of the actual to initial amplitude is important), but the same does not apply for a nonlinear wave. In the simulations, initial amplitude is 2 % of the liquid depth. The overall trend of wave fronts is qualitatively the same in both cases. In Figs. 10a, b interference holds either inside

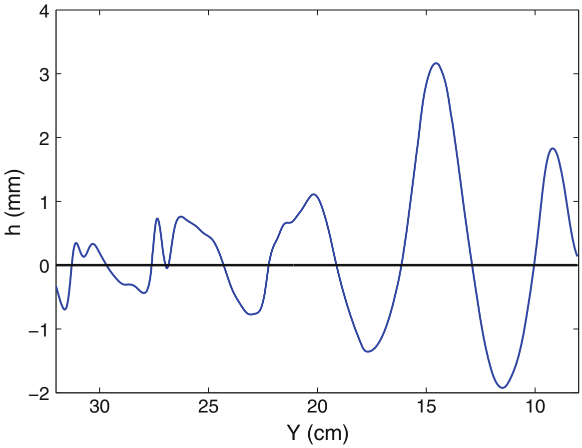

Fig. 9 Monochromatic wave of frequency f = 7 Hz along the symmetry axis. Before y = 15 cm the wave amplitude grows monotonically, but after this position there are important modification in wave, for instance around the peaks located approximately at y = 26 cm and y = 30 cm we found two local maxima

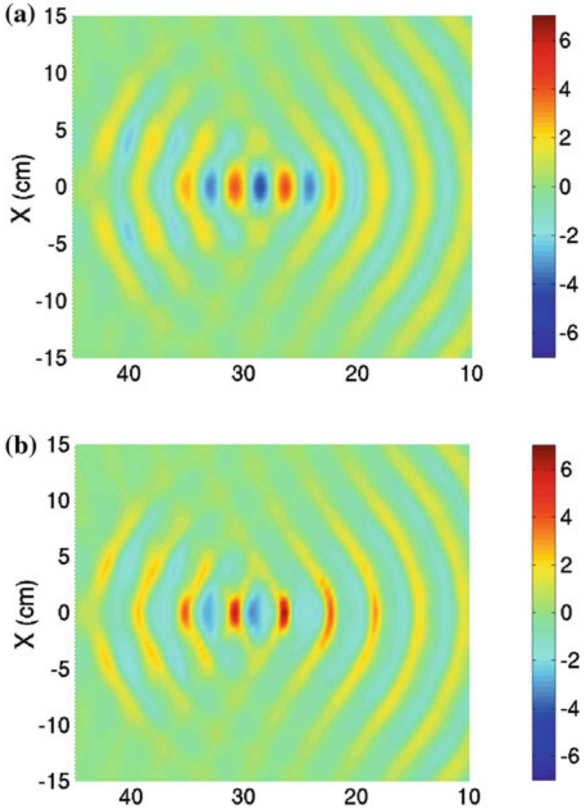

Fig. 10 Wave field of a monochromatic wave of f = 7 Hz produced by a parabolic wave maker. **a** Linear wave and **b** nonlinear wave with an initial amplitude of 2 % of the liquid depth. Wave progresses from *right* to *left*. In the figure the maximal amplitude occurs after passing the cusp. Maximal amplitude for non linear wave is greater with respect the linear wave

and outside the caustics. In the same manner, after passing the Huygens cusp, the amplitude decreases because wave becomes divergent. However some differences must be highlighted. A first thing to emphasize is that the peaks around the cusp

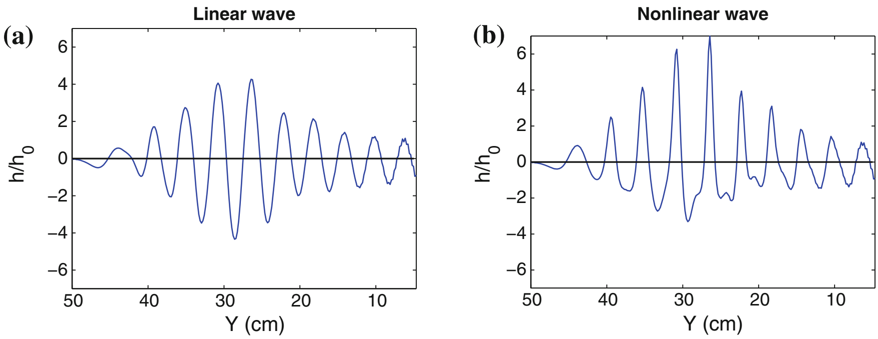

Fig. 11 Wave of frequency 7 Hz along the symmetry axis produced by a parabolic wave maker. Maximal amplitude attained by non linear wave is greater than those of the linear wave. In addition, peaks and troughs are clearly asymmetric. In the figure the maximal amplitude occurs after passing the cusp. **a** Linear wave. **b** Nonlinear wave

becomes narrower for the non linear wave if compared with the linear one. This is a proof that peaks became steeper as already seen in experiments.

A better way to see the focusing and the nonlinear behavior is to plot a wave along the symmetry axis. This is made in Fig. 11 for waves considered in Fig. 10. The first thing to remark that the linear wave is symmetric everywhere. Concerning the nonlinear wave, as already stated, we have a maximal amplitude higher than those attained in the linear case. In addition, the asymmetries between peaks and troughs are very clear. We are still far from wave breaking but nonlinear effects are already present. Instead of showing a particular wave profile, a way to see the overall behavior

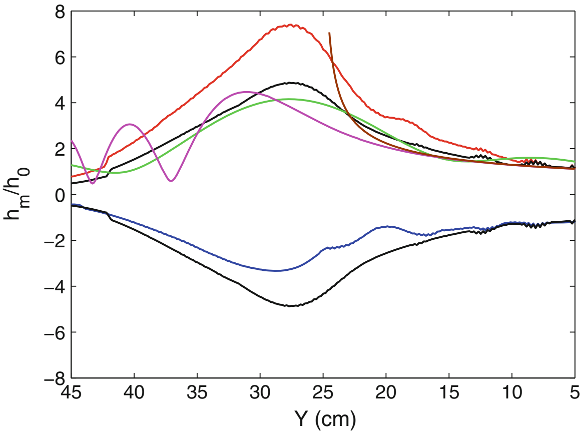

Fig. 12 Wave envelope calculated in different cases: (i) Linear wave (*black line*), (ii) nonlinear wave with initial amplitude 0.02H (*red* and *blue lines*), (iii) Pearcey integral for a finite wave maker (*green line*), (iv) Pearcey integral for an infinite wave maker (*magenta line*) and (v) envelope obtained with the stationary phase method (*brown line*). In the nonlinear case, positive and negative branches are clearly different

is to plot the wave envelope along the symmetry axis. In Fig. 12, we plot envelopes in the following cases: (i) linear wave, (ii) non linear wave with initial amplitude 0.02H., (iii) Pearcey prediction for a finite size wave maker, (iv) Pearcey prediction for an infinite wave maker, (v) envelope predicted by the stationary phase method. In all cases amplitudes are normalized with initial amplitude (h_0). It is important to point out that interference in the region inside the caustics leads to oscillations of the envelope. These oscillation are predicted by the Pearcey results. However, in a wave field produced by a finite wave maker these oscillations are less important because the zone where three rays reach a point is only a fraction of the area limited by the caustics. Far from the cusp, and according to ray theory, only a ray reaches each point. In this figure the asymmetries related with nonlinearities are evident. First, the negative branch of linear wave envelope is exactly the reflection of the positive one (black lines). The same does not apply for the non linear wave and only far from the cusp both branches becomes symmetric.

Caustics are fictitious singularities appearing in the ray theory. On the other side, dislocations are a kind of singularity which remains beyond the geometrical optics. They are points of full destructive interference and can be recognized by two facts: the wave amplitude is always zero and the phase is undetermined. According to the last feature, in a dislocation the contours of constant phase cross. The Fig. 13 shows both a diagram of the wave amplitude and curves of constant phase, calculated with the Pearcey integral. The ray theory predicts that dislocations occurs only inside the caustics, but due to diffraction two dislocations outside the caustics appear. The numerical solution of wave equation (linear and nonlinear) predicts also the existence of dislocations outside the caustics as we can see in Fig. 14, where wave amplitude as a function of (x, y) is shown. Dislocations are located in the blue regions of each

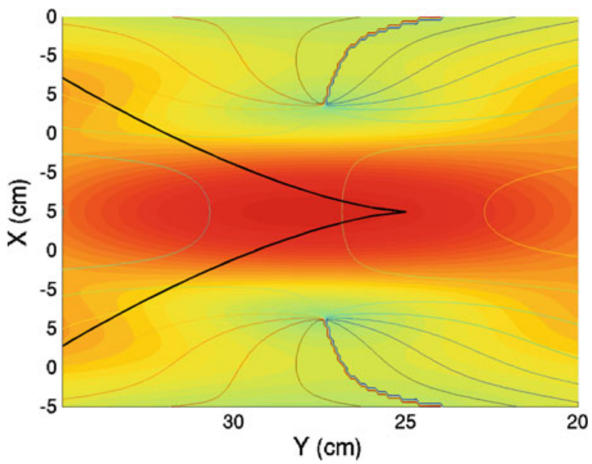

Fig. 13 Graph of wave amplitude and *curves* of constant phase obtained from the Pearcey integral, assuming a finite wave maker. The phase is undetermined in the points of full destructive interference. Then the *curves* of constant phase cross in such points. These singularities are known as dislocations

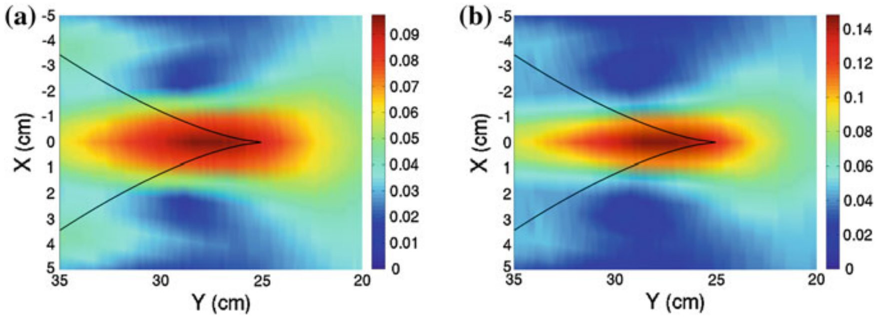

Fig. 14 Graph of the wave amplitude obtained from numerical simulation. **a** Linear case and **b** non linear case. Two dislocations appear outside the caustics both in linear and in nonlinear waves. They are located inside the *blue region* of each figure

figure, they are symmetrically situated around $x = 0$. The dislocations are located at $(-2.3, 28.9)$ and at $(2.3, 28.9)$ for the linear wave. For the nonlinear wave the dislocations are located at $(-3, 29.5)$ and at $(3, 29.5)$.

6 Conclusions

In this paper we have performed an experimental and numerical study of the wave field having three types of singularities: caustics, wave breaking and dislocations. The first one is a fictitious singularity appearing in the ray theory. It disappears when wave properties are taken into account, but its position reveals bright regions. The second kind of singularity (wave breaking) is produced by non linear interactions. In our experiments the breaking is produced through spatial focusing over a distance of some wavelengths. The wave breaking modify the shape of wave fronts and produces a dissipation of the energy. Finally, the third kind of singularities are the dislocations, which are defined as points of complete destructive interference. The singularity deals with the fact that in a dislocation phase is undefined. The experiments and numerical simulations were conducted to enhance the nonlinear effects. This research is in the first stage. A more complete research of singularities requires, among others, a detailed study of conditions of wave breaking, the determination of the amount of energy dissipated and the study of dislocations both inside and outside the caustics.

Acknowledgments G. Ruíz Chavarría acknowledges DGAPA-UNAM by support for a sabbatical period at IRPHE between September 2010 and August 2011. Additionally the authors acknowledge support by DGAPA-UNAM under project 116312, Vorticidad y ondas no lineales en fluidos. Authors acknowledge also Eric Falcon from University Paris Diderot for his assistance in the implementation of the Fourier Transform Profilometry.

References

Babanin A (2011) Breaking and dissipation of the ocean surface waves. Cambridge University Press, Cambridge

Cobelli PJ, Maurel A, Pagneux V, Petitjeans P (2009) Global measurement of water waves by Fourier transform profilometry. Exp Fluids 46:1037–1047

Elmore WC, Heald MA (1969) Phys waves. McGraw Hill, New York

Maurel A, Cobelli PJ, Pagneux V, Petitjeans P (2009) Experimental and theoretical inspection of the phase to height relation in Fourier transform profilometry. Appl Opt 48:380–392

Meunier P, Leweke T (2003) Analysis and minimization of errors due to high gradients in particle image velocimetry. Exp Fluids 35:408–421. https://www.irphe.fr/meunier/PIV

Moisy F, Rabaud M, Salsac K (2009) A synthetic Schlieren method for the measurement of the topography of a liquid surface. Exp Fluids 46:1021–1036

Paris RB, Kaminsky D (2001) Asymptotic Mellin-Barnes integrals. Cambridge University Press, Cambridge

Pearcey I (1946) The structure of an electromagnetic field in the neighborhood of a cusp of a caustic. Philos Mag 37:311–317

Ruiz-Chavarria G, Le Bars M, Le Gal P (2014) Focusing of surface waves in experimental and computational fluid mechanics. 315–325. ISSN 1431-2492

Zemenzer S (2011) Etude experimentale du deferlement des vagues en eau profonde par focalisation spatiale; Rapport de stage, Universite de la Mediterranee